
MLLMs Know When Before Speaking: Revealing and Recovering Temporal Grounding via Attention Cues

Dazhao Du^{1,3*}Liao Duan^{1,2*}Jian Liu¹Tao Han¹Yujia Zhang³Eric Liu³Xi Chen³Song Guo^{1†}¹Hong Kong University of Science and Technology ²Xi'an Jiaotong University ³Tencent

Abstract

Video temporal grounding (VTG), which localizes the start and end times of a queried event in an untrimmed video, is a key test of whether multimodal large language models (MLLMs) understand not only what happens but also when it happens. Although modern MLLMs describe video content fluently, their timestamp predictions remain unreliable, while existing remedies either require costly post-training on temporal annotations or rely on coarse training-free heuristics. In this work, we probe the cross-modal attention of MLLMs and uncover a perception-generation gap. Our key finding is that MLLMs often know the target interval during prefill, but lose this signal when generating the final answer. In the prefill stage, a sparse set of attention heads, which we call *Temporal Grounding Heads* (TG-Heads), concentrates query-to-video attention on the ground-truth interval. During autoregressive decoding, however, the answer tokens shift attention away from this interval toward visually salient but query-irrelevant segments. This observation motivates an inference-time read-then-regenerate framework. We first convert TG-Head prefill attention into a debiased frame-level relevance signal and extract the high-attention interval it highlights. We then re-invoke the MLLM with visual context restricted to this interval, using video cropping or attention masking to suppress distractors. Without parameter updates and architectural changes, our framework consistently improves MiMo-VL-7B, Qwen3-VL-8B, and TimeLens-8B on three VTG benchmarks, with gains of up to +3.5 mIoU. The project website can be found at <https://ddz16.github.io/mllmsknowwhen.github.io/>.

1 Introduction

Multimodal large language models (MLLMs) have become remarkably capable video understanders [35, 18, 7, 2], yet a simple follow-up question often trips them up: *when does it happen?* Video temporal grounding (VTG), which requires predicting the start and end times of a queried event in an untrimmed video, remains a persistent weakness of general-purpose MLLMs [27]. Existing remedies expose an uncomfortable trade-off. Post-training methods improve VTG by fitting models on large temporal-annotation corpora [37, 26, 34, 5], but require expensive annotations and specialized training pipelines. Training-free alternatives avoid this cost, but typically replace temporal localization with indirect surrogates such as segment-caption matching or numeric frame reading, sacrificing fine-grained boundary precision [39, 28, 31]. This raises the question that motivates our work: *do MLLMs genuinely lack temporal grounding ability, or do they already possess it in a latent form that standard decoding fails to surface?*

*Equal contribution. Part of this work was done while Dazhao was an intern at Tencent and Liao was a RA at HKUST.

†Corresponding author.

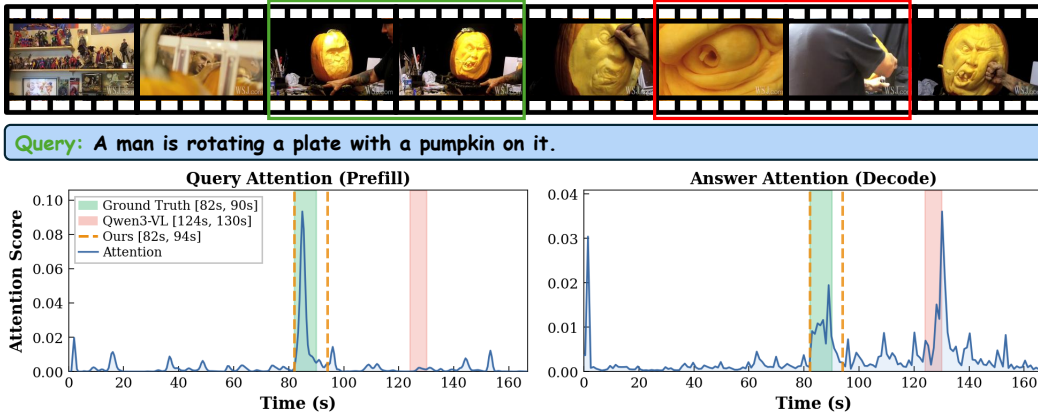


Figure 1: **MLLMs know *when* during prefill but forget during decoding.** We visualize Qwen3-VL’s cross-modal attention at inference. During prefill (left), attention from query tokens peaks at the ground-truth interval. During decoding (right), attention from the generated answer tokens drifts away to a visually salient but query-irrelevant segment, which aligns with the model’s erroneous prediction. Our method leverages the clean prefill signal to correct the final output.

To test this possibility, we first ask where a latent temporal signal would reside inside the model. Recent studies suggest that attention heads in MLLMs often specialize into distinct functional roles [13, 1, 4, 11]. We therefore conduct a systematic *head knockout* study [38, 9]: for each head, we suppress its query-to-video attention and measure the resulting drop in VTG accuracy. The result is sharply non-uniform. Out of hundreds of heads, only a small subset causes a substantial degradation when removed (Figure 2). We call them *Temporal Grounding Heads* (TG-Heads). This intervention evidence suggests that MLLMs do contain an internal temporal localization mechanism, but that it is concentrated in a sparse set of heads rather than distributed uniformly across the network.

Having located TG-Heads, we next ask how their signal is used during inference. We compare their cross-modal attention at two stages: *prefill*, where query tokens attend over the video, and *autoregressive decoding*, where newly generated answer tokens attend back to the same visual context. This reveals a clear perception-generation gap (Figure 1). During prefill, TG-Head attention from query tokens concentrates on the ground-truth interval, suggesting that the relevant frames have already been identified. During decoding, however, attention from the numeric answer tokens shifts away from this interval toward visually salient but query-irrelevant segments, and the final timestamp follows this misdirected attention. Additional examples are provided in Appendix A. This kind of disconnect between internal visual evidence and final output echoes recent observations in image VLMs [22, 36], but here it appears along the temporal axis of video.

We hypothesize that this gap arises from an asymmetry between reading and speaking. During prefill, the full query provides a focused linguistic intent, allowing TG-Heads to bind discriminative words and actions to a small set of relevant frames. During decoding, the model instead generates timestamp tokens, whose numeric form provides little semantic guidance while still attending over hundreds of visual tokens. The localized signal established by TG-Heads is therefore diluted within a much larger visual context and can be overwhelmed by salient distractors. The model knows *when*, but forgets at the moment it has to speak.

This diagnosis suggests a direct intervention: read out the clean prefill signal before it is lost, and let the model speak again after the distracting visual context has been removed. We instantiate this idea as an inference-time *read-then-regenerate* framework. Stage 1 extracts and refines the TG-Head prefill attention to detect a high-attention temporal interval. Stage 2 re-invokes the MLLM with visual context restricted to the detected interval, either by cropping the video (*Hard Crop*) or by masking out-of-interval frames while preserving the original timeline (*Soft Mask*). A confidence gate skips this second stage when the original prediction is already confident enough or aligns with the attention evidence. Across MiMo-VL-7B, Qwen3-VL-8B, and TimeLens-8B on three TimeLens-Bench datasets [37], our method consistently improves VTG performance by up to +3.5 mIoU, without parameter updates or architectural changes.

Our contributions are summarized as follows:

- We identify *Temporal Grounding Heads*, a sparse subset of attention heads whose query-to-video prefill attention provides intervention-backed evidence of latent temporal localization inside MLLMs.
- Through these heads, we reveal a perception-generation gap on VTG: the model knows the correct interval during prefill but is distracted by irrelevant frames during decoding.
- Motivated by this diagnosis, we propose an inference-time *read-then-regenerate* framework that recovers this hidden signal and improves three MLLMs on three TimeLens-Bench datasets without parameter updates or architectural changes.

2 Related Work

MLLMs for Temporal Grounding. Existing work on video temporal grounding with MLLMs can be broadly divided into post-training and training-free paradigms. *Post-training* methods [5, 6] either introduce specialized architectural components for temporal encoding, such as the learnable timestamp modality in Tempo-R0 [33] or the 1D temporal convolutions in TimeSuite [34], or rely on large-scale supervised fine-tuning and reinforcement learning on VTG corpora [21, 26, 25]. A recent representative is TimeLens [37], which post-trains MLLMs on a re-annotated 100K corpus with thinking-free RLVR. Although effective on VTG benchmarks, post-training incurs substantial annotation and compute costs and can degrade general video understanding. *Training-free* methods [39, 31] avoid these costs but often rely on indirect cues: ChatVTG [23] and VTG-GPT [30] reformulate VTG as text-level matching between query and segment captions, while Number-it [28] burns numeric watermarks onto frames and turns temporal prediction into OCR-style reading. These approaches convert continuous temporal localization into discrete or coarse-grained surrogates, which can limit boundary precision. In contrast, our method uses the model’s own cross-modal attention as an internal temporal cue: after one-time TG-Head identification, it performs inference-time read-then-regenerate without parameter updates or architectural changes, yielding fine-grained localization and consistently improving both general-purpose MLLMs and the VTG-tuned TimeLens model.

Attention Analysis in MLLMs. A growing body of work studies the internal attention of MLLMs and finds that it often reflects the correct cross-modal grounding even when the final output is wrong [22, 36]. Further analyses reveal that this visual information is not uniformly distributed across the network, but is instead carried by a sparse set of functional heads that specialize in distinct semantic roles, such as text-image alignment [4, 11, 14], OCR-like reading [1], and spatial grounding [13]. In the video domain, deep attention layers have been observed to encode query-conditioned keyframe priors [20], suggesting that MLLMs may already contain a latent temporal grounding signal. How to reliably extract and exploit this signal for precise boundary prediction, however, remains open. We address this gap by identifying *Temporal Grounding Heads* via a systematic head knockout study [38, 9] and translating their attention into explicit temporal intervals without any additional training.

3 Temporal Grounding Head

Recent studies have shown that internal attention in MLLMs exhibits clear functional specialization, with different heads playing different roles [13, 4, 11, 1]. Motivated by these observations, we ask whether temporal grounding is likewise supported by a specific subset of heads. To find out, we probe each head in the MLLM with *attention knockout*: we block the cross-modal attention flow through a single head and measure how much the grounding performance drops. Heads whose removal causes a disproportionate degradation are flagged as the functional units responsible for temporal localization.

Attention knockout. Let the MLLM have L layers and H heads per layer. For head h at layer ℓ , the attention weights are computed as

$$\mathbf{A}^{\ell,h} = \text{softmax}\left(\frac{\mathbf{Q}^{\ell,h}(\mathbf{K}^{\ell,h})^\top}{\sqrt{d_k}} + \mathbf{M}^{\ell,h}\right), \quad (1)$$

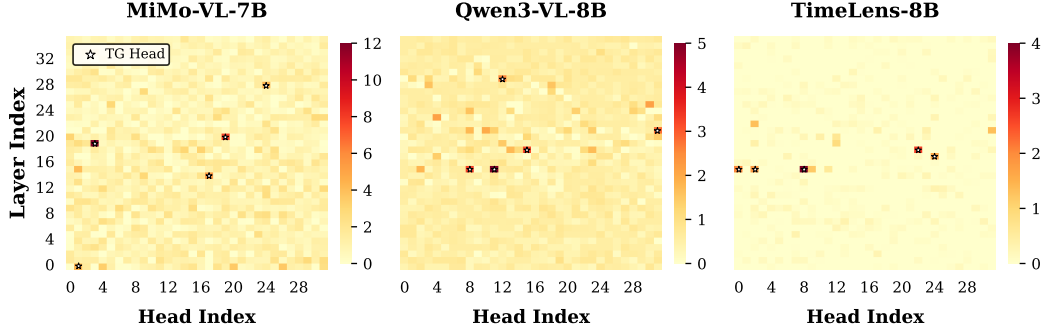


Figure 2: **Grounding Contribution Score (GCS) of each attention head** across three MLLMs. Each dot is one head, and the top- K heads are marked with stars.

where $\mathbf{Q}^{\ell,h}$ and $\mathbf{K}^{\ell,h}$ are the query and key matrices of head (ℓ, h) , d_k is the per-head feature dimension that normalizes the dot-product magnitude, and $\mathbf{M}^{\ell,h}$ is an additive mask with the same shape as $\mathbf{Q}^{\ell,h}(\mathbf{K}^{\ell,h})^\top$ that controls which attention edges are allowed. In a standard autoregressive transformer, $\mathbf{M}^{\ell,h}$ is the causal mask, i.e., $\mathbf{M}_{s,t}^{\ell,h} = 0$ if $t \leq s$ and $-\infty$ otherwise, which prevents each position from attending to future positions.

Inspired by prior attention-knockout analyses of LLMs and MLLMs [38, 9], we selectively block the cross-modal attention edges from query (text) positions to video positions for a single head. Let $\mathcal{T} = [Q_s, Q_e]$ denote the set of query-token positions and $\mathcal{S} = [V_s, V_e]$ denote the set of video-token positions. To knock out head (ℓ, h) , we modify its attention mask to:

$$\widetilde{\mathbf{M}}_{s,t}^{\ell,h} = \begin{cases} -\infty, & \text{if } t > s, \\ -\infty, & \text{if } s \in \mathcal{T} \text{ and } t \in \mathcal{S}, \\ 0, & \text{otherwise,} \end{cases} \quad (2)$$

while keeping all other heads unchanged. Recall that s indexes the query (row) dimension and t the key (column) dimension. The first case is the standard causal constraint. The second sets the attention from any query-text position $s \in \mathcal{T}$ to any video position $t \in \mathcal{S}$ to zero after softmax, surgically removing the cross-modal information flow through this head without disturbing intra-modal attention.

Measuring each head’s contribution. Intuitively, if a head is truly important for temporal localization, then blocking its cross-modal attention edges should make the model’s grounding predictions noticeably worse. Conversely, if a head is irrelevant (or even noisy) for this task, blocking it should have little effect, or may even slightly improve accuracy. We therefore quantify the contribution of each head by how much grounding performance drops when that single head is knocked out. Concretely, we evaluate the MLLM on a held-out VTG validation subset and measure the mean Intersection over Union (mIoU): let $\mathcal{M}_{\text{base}}$ be the mIoU of the intact model, and let $\mathcal{M}_{\ell,h}$ be the mIoU obtained after applying Eq. (2) to head (ℓ, h) . We define the *Grounding Contribution Score* of head (ℓ, h) as the resulting mIoU drop:

$$\text{GCS}_{\ell,h} = \mathcal{M}_{\text{base}} - \mathcal{M}_{\ell,h}. \quad (3)$$

A large positive $\text{GCS}_{\ell,h}$ means that the model heavily relies on head (ℓ, h) for temporal grounding, whereas a near-zero or negative value means the head carries little temporal grounding information.

TG-Head selection. Figure 2 visualizes $\text{GCS}_{\ell,h}$ across the full $L \times H$ grid for three MLLMs. In every model, the distribution is sharply heavy-tailed: the vast majority of heads yield near-zero or even slightly negative GCS, while only a small number of heads contribute substantially. The long-tailed pattern is also confirmed by the sorted pruning curves in Appendix G. This confirms the existence of a highly specialized subset of heads dedicated to temporal grounding. We therefore simply select the top- K heads with the highest GCS as our *Temporal Grounding Heads* (TG-Heads). Importantly, this identification is a one-time calibration requiring only a minimal probing set (e.g., 500 samples, merely 0.5% of typical VTG training corpora; see Appendix B).

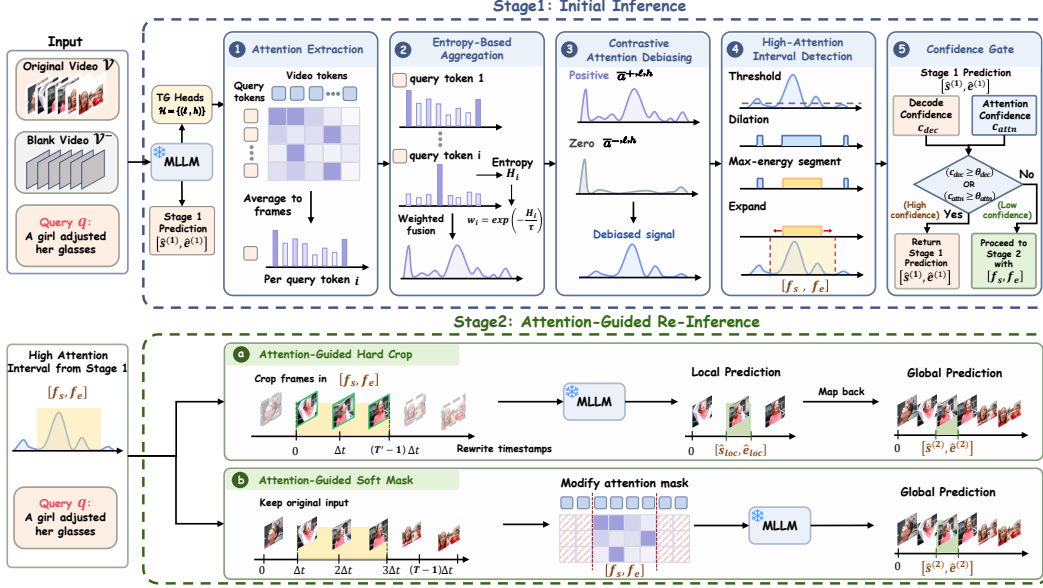


Figure 3: **Overview of our two-stage framework.** **Stage 1** runs the MLLM once to obtain a baseline prediction $[\hat{s}^{(1)}, \hat{e}^{(1)}]$ and, in parallel, processes the prefill attention of the TG-Heads through (1) extraction, (2) entropy-based aggregation, (3) contrastive debiasing against a blank-video reference, and (4) high-attention interval detection. (5) A confidence gate decides whether the baseline prediction is already reliable. **Stage 2** re-invokes the MLLM with its visual context restricted to the detected interval $[f_s, f_e]$, via either (a) Hard Crop (re-read the cropped clip) or (b) Soft Mask (hide out-of-interval visual tokens through the attention mask).

4 Inference-Time Read-Then-Regenerate with Attention Cues

Given a video \mathcal{V} of duration D consisting of T sampled frames $\{v_1, \dots, v_T\}$, and a natural language query $q = (q_1, \dots, q_M)$ of length M , our goal is to predict a temporal interval $[\hat{s}, \hat{e}] \subset [0, D]$ that localizes the queried event. Let $\Delta t = D/T$ denote the per-frame duration. Let $\mathcal{H} = \{(\ell_1, h_1), \dots, (\ell_K, h_K)\}$ denote the set of K TG-Heads identified in Section 3. Our framework proceeds in two stages.

4.1 Stage 1: Initial Inference

Attention extraction. We perform a single forward pass of the MLLM on (\mathcal{V}, q) . This pass has two outputs. First, by letting the MLLM greedily decode an answer and parsing the emitted numeric tokens, we obtain a *Stage 1 prediction* $[\hat{s}^{(1)}, \hat{e}^{(1)}] \subset [0, D]$. Second, during the prefill stage of this same pass, we read out the cross-modal attention weights from each TG-Head $(\ell, h) \in \mathcal{H}$. Following Eq. (1) with the standard causal mask, we denote the full attention weights at head (ℓ, h) by $\mathbf{A}^{\ell, h}$. Slicing the rows corresponding to the query-token positions $\mathcal{T} = [Q_s, Q_e)$ and the columns corresponding to the video-token positions $\mathcal{S} = [V_s, V_e)$ yields the query-to-video attention:

$$\mathbf{A}_{q \rightarrow v}^{\ell, h} = \mathbf{A}_{\mathcal{T}, \mathcal{S}}^{\ell, h} \in \mathbb{R}^{M \times N_v}, \quad (4)$$

where $N_v = |\mathcal{S}|$ is the total number of video tokens. Each row of $\mathbf{A}_{q \rightarrow v}^{\ell, h}$ is the attention distribution of one query token over all video tokens.

Entropy-based attention aggregation. To obtain a single frame-level curve that measures the query-video relevance, we need to reduce $\mathbf{A}_{q \rightarrow v}^{\ell, h}$ along two axes. Along the video-token axis, we simply average the attention values of all visual tokens belonging to the same frame, yielding a query-token-to-frame distribution $\mathbf{a}_i^{\ell, h} \in \mathbb{R}^T$ for each query token i . Along the query-token axis, the M distributions are however not equally informative: function words such as “a” or “the” spread attention almost uniformly over the video, while content words (nouns, verbs) concentrate attention on the

semantically relevant frames (see Appendix D). Uniformly averaging over all M rows would therefore be dominated by the uninformative ones. We instead weight each row by the negative exponential of its entropy: we normalize $\mathbf{a}_i^{\ell,h}$ to a probability distribution, compute its Shannon entropy H_i , and assign the weight $w_i = \exp(-H_i/\tau)$ with temperature $\tau=0.5$. This up-weights concentrated (low-entropy) rows and down-weights diffuse (high-entropy) ones. The fused query-video relevance curve for head (ℓ, h) is:

$$\bar{\mathbf{a}}^{\ell,h}(j) = \frac{\sum_{i=1}^M w_i \mathbf{a}_i^{\ell,h}(j)}{\sum_{i=1}^M w_i}, \quad j = 1, \dots, T. \quad (5)$$

Contrastive attention debiasing. Even after entropy-based aggregation, the curve $\bar{\mathbf{a}}^{\ell,h}$ still contains spurious peaks that are not driven by query-specific content. A representative example is the *attention sink* [32, 12]: irrespective of the query, MLLMs consistently allocate a large fraction of attention to a few positional anchors such as the first visual tokens of the video, which can dominate the detected interval (see Appendix E). To remove such content-independent biases, we borrow the idea of contrastive decoding [17]: the bias part is isolated by running the same procedure on a reference input that carries no semantic content, and subtracted from the original signal. Concretely, we replace all pixel values of \mathcal{V} with zeros to obtain a blank video \mathcal{V}^- , run a second forward pass on (\mathcal{V}^-, q) , and apply the same token-to-frame and entropy aggregation procedure, yielding a *zero-video* curve $\bar{\mathbf{a}}^{-,\ell,h}$. We denote the curve obtained from the original video (Eq. 5) as $\bar{\mathbf{a}}^{+,\ell,h}$. Both curves are Gaussian-smoothed and L_1 -normalized. The per-head debiased signal is then the pointwise positive log-ratio:

$$\mathbf{s}^{\ell,h}(j) = \max\left(\bar{\mathbf{a}}^{+,\ell,h}(j) \log \frac{\bar{\mathbf{a}}^{+,\ell,h}(j)}{\bar{\mathbf{a}}^{-,\ell,h}(j)}, 0\right), \quad (6)$$

which retains only the frames where the positive video has higher attention than what the bias alone would predict. Finally, we fuse across the K TG-Heads by a simple average:

$$\mathbf{s}(j) = \frac{1}{K} \sum_{(\ell,h) \in \mathcal{H}} \mathbf{s}^{\ell,h}(j). \quad (7)$$

The resulting $\mathbf{s} \in \mathbb{R}^T$ is the single debiased frame-level relevance signal used below.

High-attention interval detection. From \mathbf{s} we extract a temporal interval that captures the query-relevant region. We adopt a simple threshold-then-dilate routine, analogous to how prior work extracts spatial bounding boxes from VLM attention maps via thresholding and connected-region analysis [13], but adapted to the 1D temporal axis. The routine has four steps. First, we binarize the signal by keeping frames where $\mathbf{s}(j) \geq \rho \cdot \max_j \mathbf{s}(j)$. Second, we perform 1D morphological dilation with a window of $\lceil \delta/\Delta t \rceil$ frames, which sets a frame to active whenever any frame within the window is active, thereby bridging short gaps between nearby active regions that likely belong to the same event. Third, among the resulting connected segments we select the one with the largest cumulative energy $\sum_{j \in \text{seg}} \mathbf{s}(j)$. Finally, we expand the chosen segment by a fraction r of its length on each side (clamped to $[1, T]$) to provide temporal context. The output is the frame interval $[f_s, f_e] \subset [1, T]$, corresponding to the time interval $[(f_s - 1)\Delta t, f_e \Delta t]$.

Confidence gate. Finally, we estimate whether the Stage 1 prediction $[\hat{s}^{(1)}, \hat{e}^{(1)}]$ already aligns with the attention signal, in which case Stage 2 is unnecessary. We compute two complementary confidence scores. The *decode confidence* c_{dec} is the geometric mean of the softmax probabilities of all numeric tokens emitted during Stage 1 greedy decoding: $c_{\text{dec}} = \exp(\frac{1}{|\mathcal{N}|} \sum_{i \in \mathcal{N}} \log p_i)$, where \mathcal{N} is the set of numeric-token positions in the generated answer and p_i is the softmax probability of the chosen token at position i . The *attention confidence* c_{attn} measures whether the predicted region already contains the attention peak: $c_{\text{attn}} = \max_{j \in [\hat{f}_s^{(1)}, \hat{f}_e^{(1)}]} \mathbf{s}(j) / \max_j \mathbf{s}(j)$, where $[\hat{f}_s^{(1)}, \hat{f}_e^{(1)}]$ is the frame interval corresponding to the Stage 1 prediction (in the rare case where $\max_j \mathbf{s}(j) = 0$, we set $c_{\text{attn}} = 0$). If either score exceeds its threshold, $c_{\text{dec}} \geq \theta_{\text{dec}}$ or $c_{\text{attn}} \geq \theta_{\text{attn}}$, we skip Stage 2 and return the Stage 1 prediction. Otherwise, we proceed to Stage 2 with $[f_s, f_e]$ as the guidance interval.

4.2 Stage 2: Attention-Guided Re-Inference

When the confidence gate concludes that the Stage 1 prediction is unreliable, we ask the MLLM to regenerate its answer while restricting its visual context to the high-attention interval $[f_s, f_e]$.

Table 1: **Main Results.** “+Ours” denotes applying our inference-time framework to the backbone above. Gains are shown in green (†). Entries marked with * are taken from the TimeLens paper [37]. The rest are our reproductions under the same protocol.

Model	QVHighlights-TimeLens				Charades-TimeLens				ActivityNet-TimeLens			
	R1@0.3	R1@0.5	R1@0.7	mIoU	R1@0.3	R1@0.5	R1@0.7	mIoU	R1@0.3	R1@0.5	R1@0.7	mIoU
<i>Proprietary Models</i>												
GPT-4o* [10]	69.0	54.8	38.5	52.1	60.6	44.5	23.5	41.8	55.2	41.4	25.8	40.4
GPT-5* [24]	72.4	60.4	46.4	56.8	59.3	42.0	22.0	40.5	57.4	44.9	30.4	42.9
Gemini-2.0-Flash* [7]	76.2	66.4	48.3	60.8	66.4	53.5	27.1	46.7	62.9	54.0	37.7	49.3
Gemini-2.5-Flash* [7]	78.2	69.4	55.0	64.3	68.7	56.1	30.6	48.6	66.8	57.5	41.3	52.5
Gemini-2.5-Pro* [7]	84.1	75.9	61.1	70.4	74.1	61.1	34.0	52.8	72.3	64.2	47.1	58.1
<i>Open-Source Models</i>												
VideoChat-Flash-7B* [18]	45.2	30.6	16.7	32.7	60.2	37.9	17.8	39.7	35.5	21.8	10.5	24.8
VideoChat-R1-7B* [19]	29.3	19.1	9.4	21.5	51.9	30.8	11.7	33.7	35.0	23.9	11.3	25.0
Time-R1-7B* [26]	65.8	51.5	36.1	49.2	57.9	32.0	16.9	36.6	44.8	31.0	19.0	33.1
TimeSuite* [34]	27.1	16.9	9.9	21.7	56.3	35.5	18.0	38.1	27.1	17.5	8.6	19.8
Grounded-VideoLLM* [25]	43.7	33.8	22.5	33.4	43.3	28.7	13.5	30.0	39.2	29.6	19.5	30.0
Qwen2.5-VL-7B [3]	44.1	31.5	17.1	33.7	60.4	38.0	16.8	39.8	45.6	32.0	17.0	32.5
MiMo-VL-7B [29]	65.1	55.4	40.9	51.8	63.8	46.5	24.4	44.4	58.3	45.8	29.2	42.6
MiMo-VL-7B (+Ours)	70.1 ^{†5.0}	58.9 ^{†3.5}	43.5 ^{†2.6}	55.3 ^{†3.5}	65.0 ^{†1.2}	48.4 ^{†1.9}	25.9 ^{†1.5}	46.0 ^{†1.6}	59.6 ^{†1.3}	47.6 ^{†1.8}	30.4 ^{†1.2}	44.1 ^{†1.5}
Qwen3-VL-8B [2]	74.1	64.1	49.1	59.4	69.0	53.1	27.6	48.2	62.2	51.6	34.7	46.9
Qwen3-VL-8B (+Ours)	77.3 ^{†3.2}	67.0 ^{†2.9}	51.2 ^{†2.1}	61.9 ^{†2.5}	71.2 ^{†2.2}	55.2 ^{†2.1}	28.3 ^{†0.7}	49.5 ^{†1.3}	64.2 ^{†2.0}	52.9 ^{†1.3}	35.4 ^{†0.7}	48.2 ^{†1.3}
TimeLens-8B [37]	80.1	71.5	55.5	65.4	76.6	63.0	35.2	55.2	68.7	58.0	40.8	53.1
TimeLens-8B (+Ours)	80.6 ^{†0.5}	71.9 ^{†0.4}	55.7 ^{†0.2}	65.8 ^{†0.4}	76.9 ^{†0.3}	63.4 ^{†0.4}	35.3 ^{†0.1}	55.5 ^{†0.3}	68.9 ^{†0.2}	58.2 ^{†0.2}	41.2 ^{†0.4}	53.3 ^{†0.2}

This directly addresses the perception-generation gap: the signal that the TG-Heads have already captured can no longer be washed out by query-irrelevant frames during decoding. We provide two complementary ways to realize this restriction.

Attention-guided hard crop. With a fixed total visual-token budget B distributed across all T frames, each frame receives on average B/T tokens. By re-invoking the video processor on the cropped clip spanning the $T' = f_e - f_s + 1$ frames in $[f_s, f_e]$, we obtain roughly B/T' tokens per frame, giving the MLLM a finer visual resolution on the target segment. We rewrite all frame timestamps to start from zero to match the training distribution. The MLLM then produces a local prediction $[\hat{s}_{\text{loc}}, \hat{e}_{\text{loc}}]$, which is mapped back to the original timeline by:

$$[\hat{s}^{(2)}, \hat{e}^{(2)}] = \text{clip}([\hat{s}_{\text{loc}}, \hat{e}_{\text{loc}}] + (f_s - 1)\Delta t, 0, D). \quad (8)$$

Attention-guided soft mask. Hard cropping sharpens the target segment but discards surrounding context and breaks alignment with the original timeline. An alternative is to keep the original input unchanged and surgically hide out-of-interval visual tokens at attention time. Concretely, we override the default causal mask of every attention head with $\mathbf{M}^{\ell, h}$ that additionally sets $\mathbf{M}_{s, t}^{\ell, h} = -\infty$ for all s whenever t is a visual token of a frame outside $[f_s, f_e]$. This makes out-of-interval visual tokens completely invisible in the key dimension: no position (text, timestamp, or other video token) can attend to them. Timestamp text tokens remain unmasked, preserving the original timeline for the model. The final prediction $[\hat{s}^{(2)}, \hat{e}^{(2)}]$ is therefore read out directly, with no output remapping.

5 Experiments

5.1 Experimental Setup

Datasets and metrics. We evaluate on three benchmarks from TimeLens-Bench [37], which are manually re-annotated versions of three widely-used VTG datasets: **Charades-TimeLens**, built on Charades-STA [8]; **ActivityNet-TimeLens**, built on ActivityNet Captions [15]; and **QVHighlights-TimeLens**, built on QVHighlights [16]. Together they cover a wide range of video domains, durations, and query semantics. Following standard practice [37], we report $\text{R1@}\theta$ (fraction of predictions with $\text{IoU} \geq \theta$) for $\theta \in \{0.3, 0.5, 0.7\}$ and the mean IoU (mIoU).

Table 2: **Qwen3-VL across model sizes** on QVHighlights-TimeLens. Gains are shown in green (\uparrow).

Size	4B				8B				32B			
	R1@0.3	R1@0.5	R1@0.7	mIoU	R1@0.3	R1@0.5	R1@0.7	mIoU	R1@0.3	R1@0.5	R1@0.7	mIoU
Qwen3-VL [2]	74.8	65.0	49.6	59.9	74.1	64.1	49.1	59.4	73.3	64.1	48.0	59.6
+Ours	76.1\uparrow1.3	66.0\uparrow1.0	50.4\uparrow0.8	61.0\uparrow1.1	77.3\uparrow3.2	67.0\uparrow2.9	51.2\uparrow2.1	61.9\uparrow2.5	75.4\uparrow2.1	65.9\uparrow1.8	50.5\uparrow2.5	62.0\uparrow2.4

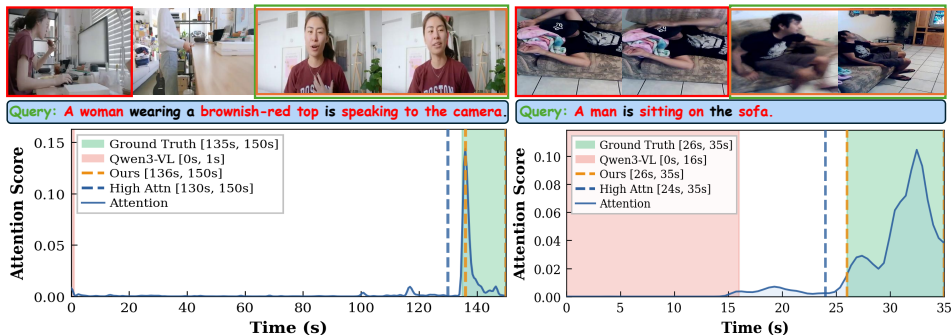


Figure 4: **Qualitative results.** Two examples where our method corrects an erroneous baseline prediction. Blue dashed boxes indicate the detected high-attention interval.

Baselines. We apply our framework to three MLLMs: **MiMo-VL-7B** [29] and **Qwen3-VL-8B** [2], which are general-purpose models not fine-tuned for VTG, and **TimeLens-8B** [37], which is post-trained from Qwen3-VL-8B on 100K VTG annotations.

Implementation details. We strictly follow the inference protocol of TimeLens [37], including the per-video total visual-token budget, the frame sampling strategy, and the prompt template, so that our reproductions are directly comparable to the numbers reported in the TimeLens paper. For all backbones we use $K=5$ TG-Heads, identified once per model by the knockout procedure of Section 3 and then fixed throughout. For Stage 2 we choose the variant based on the backbone: *Hard Crop* for the general-purpose MiMo-VL-7B and Qwen3-VL-8B, and *Soft Mask* for the VTG-tuned TimeLens-8B. Intuitively, Hard Crop benefits base models by removing query-irrelevant visual context while increasing per-frame resolution on the relevant segment, whereas TimeLens-8B has been specifically trained with the VTG corpus and works better when the original timeline and surrounding context are preserved. All experiments use greedy decoding and run on $8 \times H20$ GPUs. Complete hyperparameter settings are deferred to Appendix I.

5.2 Main Results

Main results. Table 1 summarizes the main results. Our framework delivers consistent improvements across all three backbones and all three benchmarks. The gains are especially large on QVHighlights-TimeLens, where MiMo-VL-7B improves by +3.5 mIoU and Qwen3-VL-8B by +2.5 mIoU. Even the VTG-tuned TimeLens-8B, which is already one of the strongest open-source models, benefits from our method (e.g., +0.4 mIoU on QVHighlights-TimeLens). We observe that the gains on general-purpose models are substantially larger than on TimeLens-8B. This is expected: TimeLens-8B has already been post-trained to produce accurate temporal predictions, leaving less room for improvement. In contrast, general-purpose MLLMs make more errors at Stage 1, and these errors are precisely the ones our attention-guided re-inference is designed to correct. Overall, this result supports our core claim that general-purpose MLLMs already possess a latent temporal grounding ability that can be surfaced without any training. Comparison with two representative training-free methods (Moment-GPT [31], NumPro [28]) can be found in Appendix C.

Models with Different Sizes. Table 2 reports results for Qwen3-VL at three scales (4B, 8B, 32B). The performance gap across scales is surprisingly small for VTG (the 4B model at 59.9 mIoU is on par with the 32B model at 59.6 mIoU), and our framework delivers consistent gains at every scale, confirming that it serves as a plug-and-play enhancement regardless of backbone size.

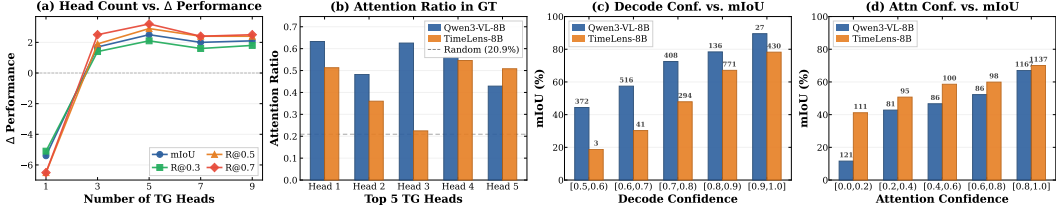


Figure 5: **Analysis on Qwen3-VL-8B and TimeLens-8B** (QVHighlights-TimeLens). (a) Performance vs. number of TG-Heads K . (b) Attention ratio of the ground-truth interval in each of the top-5 TG-Heads, compared to a random baseline (dashed line). (c, d) Stage 1 mIoU bucketed by decode confidence (c) and attention confidence (d); numbers above bars are sample counts.

Qualitative evaluation. Figure 4 visualizes two representative corrections. In the first case, a woman appears at the beginning of the video but is not speaking to the camera there. The baseline is misled by this visual similarity, while our TG-Head attention peaks at the correct later segment, and the detected high-attention interval (blue dashed boxes) excludes the distractor. In the second case, the man and sofa are present throughout the video, but the man is lying down earlier and only sits up later. The baseline confuses the two, while our high-attention interval filters out the earlier segment and guides Stage 2 to the correct prediction. Additional examples are in Appendix K.

5.3 More Analysis

Sensitivity to Attention Heads. Figure 5(a) shows performance as a function of the number of TG-Heads K . Using a single head ($K=1$) actually degrades performance, as individual heads lack sufficient coverage to reliably localize diverse events. Performance improves steadily as more heads are added, peaking at $K=5$, where multiple complementary heads jointly identify the optimal interval. Beyond $K=5$, weaker heads introduce noise that broadens the detected interval to include irrelevant regions, causing a slight decline. We therefore use $K=5$ for all experiments.

Do MLLMs Really Know When to Look? Figure 5(b) provides direct evidence. We compute the attention ratio, defined as the fraction of total attention falling within the ground-truth interval, for the top-5 TG-Heads. This ratio consistently exceeds the random baseline, confirming that TG-Heads genuinely localize queried events. Interestingly, the base Qwen3-VL exhibits higher attention ratios than the VTG-tuned TimeLens-8B. We hypothesize that VTG post-training forces TimeLens-8B’s TG-Heads to multitask: they must align visual semantics while simultaneously attending to positional tokens for exact numeric formatting. This entanglement dilutes the absolute visual attention, resulting in a lower ratio. In contrast, Qwen3-VL maintains a focused, format-free semantic-to-visual attention. Our method explicitly extracts this cleaner signal, which explains its larger gains on the base model.

The Effect of Confidence Gate. Figures 5(c,d) show that both decode confidence and attention confidence are positively correlated with mIoU. In the majority of cases, the model is confident and achieves high accuracy, indicating that its Stage 1 prediction is already reliable. However, a non-negligible fraction of samples fall into low-confidence bins, and these samples consistently correspond to poor localization. These are precisely the cases where the model’s decoding drifts away from its own attention evidence. Our confidence gate identifies them and routes them to Stage 2 for correction, while leaving the already-accurate high-confidence predictions untouched.

Ablations on Attention Aggregation. Table 3 compares four aggregation strategies on Qwen3-VL-8B. *Average* treats all query tokens equally, yielding marginal gains (+0.4 mIoU) because uninformative tokens dilute the temporal signal. *Next Token* uses the attention of the token immediately following the query, which benefits from causal self-attention over the full query context and achieves strong results (+2.1 mIoU). *Last Token* uses the final prompt token to represent the holistic query semantics. Our *entropy-based* aggregation achieves the best overall performance (+2.5 mIoU) by automatically identifying and upweighting the most temporally discriminative query tokens without requiring positional heuristics.

Table 3: **Ablation on attention aggregation strategies** (Qwen3-VL-8B, QVHighlights-TimeLens).

Method	R1@0.3	R1@0.5	R1@0.7	mIoU
Baseline	74.1	64.1	49.1	59.4
Average	75.5	64.2	48.5	59.8
Next Token	77.0	66.6	50.6	61.5
Last Token	75.2	64.9	51.0	61.2
Entropy (Ours)	77.3	67.0	51.2	61.9

6 Conclusion

We have shown that MLLMs often know *when* before they speak. By probing query-to-video attention, we identify Temporal Grounding Heads whose prefill attention concentrates on the target interval, even when the final generated timestamp is incorrect. This reveals a perception-generation gap: temporal grounding evidence is present inside the model, but can be diluted or redirected during decoding. Our inference-time read-then-regenerate framework recovers this hidden signal by converting TG-Head attention into a temporal relevance cue and using it to restrict distracting visual context before regeneration. Improvements across various MLLMs demonstrate that bridging the gap between what MLLMs internally attend to and what they ultimately generate can enhance VTG without modifying model parameters, and may benefit broader reliable multimodal reasoning.

References

- [1] Ingeol Baek, Hwan Chang, Sunghyun Ryu, and Hwanhee Lee. How do large vision-language models see text in image? unveiling the distinctive role of ocr heads. In *Proceedings of the 2025 Conference on Empirical Methods in Natural Language Processing*, pages 20452–20464, 2025.
- [2] Shuai Bai, Yuxuan Cai, Ruizhe Chen, Keqin Chen, Xionghui Chen, Zesen Cheng, Lianghao Deng, Wei Ding, Chang Gao, Chunjiang Ge, et al. Qwen3-vl technical report. *arXiv preprint arXiv:2511.21631*, 2025.
- [3] Shuai Bai, Keqin Chen, Xuejing Liu, Jialin Wang, Wenbin Ge, Sibong Song, Kai Dang, Peng Wang, Shijie Wang, Jun Tang, et al. Qwen2.5-vl technical report. *arXiv preprint arXiv:2502.13923*, 2025.
- [4] Jing Bi, Junjia Guo, Yunlong Tang, Lianggong Bruce Wen, Zhang Liu, Bingjie Wang, and Chenliang Xu. Unveiling visual perception in language models: An attention head analysis approach. In *Proceedings of the Computer Vision and Pattern Recognition Conference*, pages 4135–4144, 2025.
- [5] Ruizhe Chen, Tianze Luo, Zhiting Fan, Heqing Zou, Zhaopeng Feng, Guiyang Xie, Hansheng Zhang, Zhuochen Wang, Zuozhu Liu, and Zhang Huaijian. Datasets and recipes for video temporal grounding via reinforcement learning. In *Proceedings of the 2025 Conference on Empirical Methods in Natural Language Processing: Industry Track*, pages 983–992, 2025.
- [6] Jen-Hao Cheng, Vivian Wang, Huayu Wang, Huapeng Zhou, Yi-Hao Peng, Hou-I Liu, Hsiang-Wei Huang, Kuang-Ming Chen, Cheng-Yen Yang, Wenhao Chai, et al. Tempura: Temporal event masked prediction and understanding for reasoning in action. *arXiv preprint arXiv:2505.01583*, 2025.
- [7] Gheorghe Comanici, Eric Bieber, Mike Schaekermann, Ice Pasupat, Noveen Sachdeva, Inderjit Dhillon, Marcel Blistein, Ori Ram, Dan Zhang, Evan Rosen, et al. Gemini 2.5: Pushing the frontier with advanced reasoning, multimodality, long context, and next generation agentic capabilities. *arXiv preprint arXiv:2507.06261*, 2025.
- [8] Jiyang Gao, Chen Sun, Zhenheng Yang, and Ram Nevatia. Tall: Temporal activity localization via language query. In *Proceedings of the IEEE international conference on computer vision*, pages 5267–5275, 2017.
- [9] Chenhui Gou, Ziyu Ma, Zicheng Duan, Haoyu He, Feng Chen, Akide Liu, Bohan Zhuang, Jianfei Cai, and Hamid Rezafofighi. An empirical study on how video-llms answer video questions. *arXiv preprint arXiv:2508.15360*, 2025.
- [10] Aaron Hurst, Adam Lerer, Adam P Goucher, Adam Perelman, Aditya Ramesh, Aidan Clark, AJ Ostrow, Akila Welihinda, Alan Hayes, Alec Radford, et al. Gpt-4o system card. *arXiv preprint arXiv:2410.21276*, 2024.
- [11] Yanbei Jiang, Xueqi Ma, Shu Liu, Sarah Monazam Erfani, Tongliang Liu, James Bailey, Jey Han Lau, and Krista A Ehinger. Investigating the functional roles of attention heads in vision language models: Evidence for reasoning modules. *arXiv preprint arXiv:2512.10300*, 2025.

- [12] Seil Kang, Jinyeong Kim, Junhyeok Kim, and Seong Jae Hwang. See what you are told: Visual attention sink in large multimodal models. *arXiv preprint arXiv:2503.03321*, 2025.
- [13] Seil Kang, Jinyeong Kim, Junhyeok Kim, and Seong Jae Hwang. Your large vision-language model only needs a few attention heads for visual grounding. In *Proceedings of the Computer Vision and Pattern Recognition Conference*, pages 9339–9350, 2025.
- [14] Jinyeong Kim, Seil Kang, Jiwoo Park, Junhyeok Kim, and Seong Jae Hwang. Interpreting attention heads for image-to-text information flow in large vision-language models. *arXiv preprint arXiv:2509.17588*, 2025.
- [15] Ranjay Krishna, Kenji Hata, Frederic Ren, Li Fei-Fei, and Juan Carlos Niebles. Dense-captioning events in videos. In *Proceedings of the IEEE international conference on computer vision*, pages 706–715, 2017.
- [16] Jie Lei, Tamara L Berg, and Mohit Bansal. Detecting moments and highlights in videos via natural language queries. *Advances in Neural Information Processing Systems*, 34:11846–11858, 2021.
- [17] Xiang Lisa Li, Ari Holtzman, Daniel Fried, Percy Liang, Jason Eisner, Tatsunori B Hashimoto, Luke Zettlemoyer, and Mike Lewis. Contrastive decoding: Open-ended text generation as optimization. In *Proceedings of the 61st annual meeting of the association for computational linguistics (volume 1: Long papers)*, pages 12286–12312, 2023.
- [18] Xinhao Li, Yi Wang, Jiashuo Yu, Xiangyu Zeng, Yuhan Zhu, Haiyan Huang, Jianfei Gao, Kunchang Li, Yanan He, Chenting Wang, et al. Videochat-flash: Hierarchical compression for long-context video modeling. *arXiv preprint arXiv:2501.00574*, 2024.
- [19] Xinhao Li, Ziang Yan, Desen Meng, Lu Dong, Xiangyu Zeng, Yanan He, Yali Wang, Yu Qiao, Yi Wang, and Limin Wang. Videochat-r1: Enhancing spatio-temporal perception via reinforcement fine-tuning. *arXiv preprint arXiv:2504.06958*, 2025.
- [20] Yulin Li, Haokun Gui, Ziyang Fan, Junjie Wang, Bin Kang, Bin Chen, and Zhuotao Tian. Less is more, but where? dynamic token compression via llm-guided keyframe prior. *arXiv preprint arXiv:2512.06866*, 2025.
- [21] Yunheng Li, Jing Cheng, Shaoyong Jia, Hangyi Kuang, Shaohui Jiao, Qibin Hou, and Ming-Ming Cheng. Tempsamp-r1: Effective temporal sampling with reinforcement fine-tuning for video llms. *arXiv preprint arXiv:2509.18056*, 2025.
- [22] Zhining Liu, Ziyi Chen, Hui Liu, Chen Luo, Xianfeng Tang, Suhang Wang, Joy Zeng, Zhenwei Dai, Zhan Shi, Tianxin Wei, et al. Seeing but not believing: Probing the disconnect between visual attention and answer correctness in vlms. *arXiv preprint arXiv:2510.17771*, 2025.
- [23] Mengxue Qu, Xiaodong Chen, Wu Liu, Alicia Li, and Yao Zhao. Chatvtg: Video temporal grounding via chat with video dialogue large language models. In *Proceedings of the IEEE/CVF Conference on Computer Vision and Pattern Recognition*, pages 1847–1856, 2024.
- [24] Aaditya Singh, Adam Fry, Adam Perelman, Adam Tart, Adi Ganesh, Ahmed El-Kishky, Aidan McLaughlin, Aiden Low, AJ Ostrow, Akhila Ananthram, et al. Openai gpt-5 system card. *arXiv preprint arXiv:2601.03267*, 2025.
- [25] Haibo Wang, Zhiyang Xu, Yu Cheng, Shizhe Diao, Yufan Zhou, Yixin Cao, Qifan Wang, Weifeng Ge, and Lifu Huang. Grounded-videollm: Sharpening fine-grained temporal grounding in video large language models. *arXiv preprint arXiv:2410.03290*, 2024.
- [26] Ye Wang, Ziheng Wang, Boshen Xu, Yang Du, Kejun Lin, Zihan Xiao, Zihao Yue, Jianzhong Ju, Liang Zhang, Dingyi Yang, et al. Time-r1: Post-training large vision language model for temporal video grounding. *arXiv preprint arXiv:2503.13377*, 2025.
- [27] Jianlong Wu, Wei Liu, Ye Liu, Meng Liu, Liqiang Nie, Zhouchen Lin, and Chang Wen Chen. A survey on video temporal grounding with multimodal large language model. *IEEE Transactions on Pattern Analysis and Machine Intelligence*, 2025.

- [28] Yongliang Wu, Xinting Hu, Yuyang Sun, Yizhou Zhou, Wenbo Zhu, Fengyun Rao, Bernt Schiele, and Xu Yang. Number it: Temporal grounding videos like flipping manga. In *Proceedings of the Computer Vision and Pattern Recognition Conference*, pages 13754–13765, 2025.
- [29] LLM-Core-Team Xiaomi. Mimo-vl technical report, 2025. URL <https://arxiv.org/abs/2506.03569>.
- [30] Yifang Xu, Yunzhuo Sun, Zien Xie, Benxiang Zhai, and Sidan Du. Vtg-gpt: Tuning-free zero-shot video temporal grounding with gpt. *Applied Sciences*, 14(5):1894, 2024.
- [31] Yifang Xu, Yunzhuo Sun, Benxiang Zhai, Ming Li, Wenxin Liang, Yang Li, and Sidan Du. Zero-shot video moment retrieval via off-the-shelf multimodal large language models. In *Proceedings of the AAAI Conference on Artificial Intelligence*, volume 39, pages 8978–8986, 2025.
- [32] Zhongzhi Yu, Zheng Wang, Yonggan Fu, Huihong Shi, Khalid Shaikh, and Yingyan Celine Lin. Unveiling and harnessing hidden attention sinks: Enhancing large language models without training through attention calibration. *arXiv preprint arXiv:2406.15765*, 2024.
- [33] Feng Yue, Zhaoxing Zhang, Junming Jiao, Zhengyu Liang, Shiwen Cao, Feifei Zhang, and Rong Shen. Tempo-r0: A video-mlm for temporal video grounding through efficient temporal sensing reinforcement learning. *arXiv preprint arXiv:2507.04702*, 2025.
- [34] Xiangyu Zeng, Kunchang Li, Chenting Wang, Xinhao Li, Tianxiang Jiang, Ziang Yan, Songze Li, Yansong Shi, Zhengrong Yue, Yi Wang, et al. Timesuite: Improving mllms for long video understanding via grounded tuning. *arXiv preprint arXiv:2410.19702*, 2024.
- [35] Hang Zhang, Xin Li, and Lidong Bing. Video-llama: An instruction-tuned audio-visual language model for video understanding. In *Proceedings of the 2023 conference on empirical methods in natural language processing: system demonstrations*, pages 543–553, 2023.
- [36] Jiarui Zhang, Mahyar Khayatkhoei, Prateek Chhikara, and Filip Ilievski. Mllms know where to look: Training-free perception of small visual details with multimodal llms. *arXiv preprint arXiv:2502.17422*, 2025.
- [37] Jun Zhang, Teng Wang, Yuying Ge, Yixiao Ge, Xinhao Li, Ying Shan, and Limin Wang. Timelens: Rethinking video temporal grounding with multimodal llms. *arXiv preprint arXiv:2512.14698*, 2025.
- [38] Zhi Zhang, Srishti Yadav, Fengze Han, and Ekaterina Shutova. Cross-modal information flow in multimodal large language models. In *Proceedings of the Computer Vision and Pattern Recognition Conference*, pages 19781–19791, 2025.
- [39] Minghang Zheng, Xinhao Cai, Qingchao Chen, Yuxin Peng, and Yang Liu. Training-free video temporal grounding using large-scale pre-trained models. In *European Conference on Computer Vision*, pages 20–37. Springer, 2024.

A Additional Motivation Examples

To supplement Figure 1 in the main paper, we provide two additional motivating examples in Figures 6 and 7. Both examples reinforce the central observation that MLLMs reliably localize the queried event during prefill but drift away from this localization during autoregressive decoding.

In Figure 6, the query asks about a woman organizing wired earphones. The query attention (prefill) sharply peaks around the ground-truth interval [35s, 38s], and our method successfully predicts [35s, 42s]. In contrast, the answer attention (decoding) drifts to a later segment around [58s, 64s] where the scene is visually similar but the target action is not actually occurring, and the baseline Qwen3-VL predicts exactly this wrong interval.

Figure 7 shows a case where the answer attention is overwhelmed by the very first frame rather than by a distractor segment. The query is about a man filming himself with a video camera. While the query attention still clearly localizes the ground-truth interval [78s, 89s], the answer attention is dominated by the attention sink at the beginning of the video, and the model ends up predicting [0s, 2s]. Our method produces [78s, 83s], closely matching the ground truth.

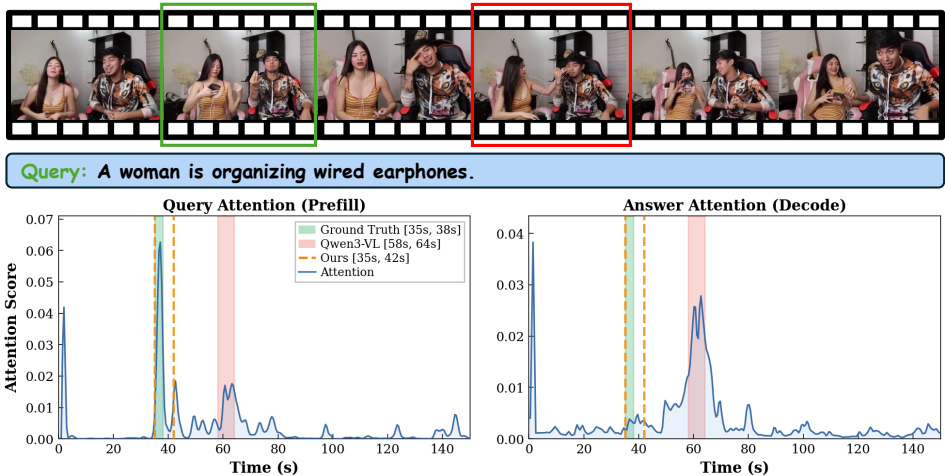


Figure 6: Additional motivation example. Query attention (prefill) correctly focuses on the ground-truth interval, while answer attention (decoding) is distracted by a visually similar but query-irrelevant later segment.

B Full Implementation Details

Throughout this work we aim for a direct comparison with TimeLens [37], so we keep the inference protocol identical to theirs whenever possible. We summarize the full details below for reproducibility.

Prompt template. We use the same grounding prompt as TimeLens [37]. The entire conversation consists of a single user turn that contains the video followed by an instruction:

User: <video>
Please find the visual event described by the sentence ‘{query}’, determining its starting and ending times. The format should be: ‘The event happens in <start time> - <end time> seconds’.

For the TimeLens-8B backbone, the video is processed using Qwen3-VL’s native interleaved timestamp mechanism, so the timestamp of every frame is automatically inserted before its visual tokens by the processor. For MiMo-VL-7B, we additionally append the /no_think suffix to disable its reasoning mode, following its official inference recipe.

Video sampling and token budget. Each video is uniformly sampled at a fixed rate (FPS) and then passed to the MLLM’s native video encoder, which packs the resulting frames into a fixed total

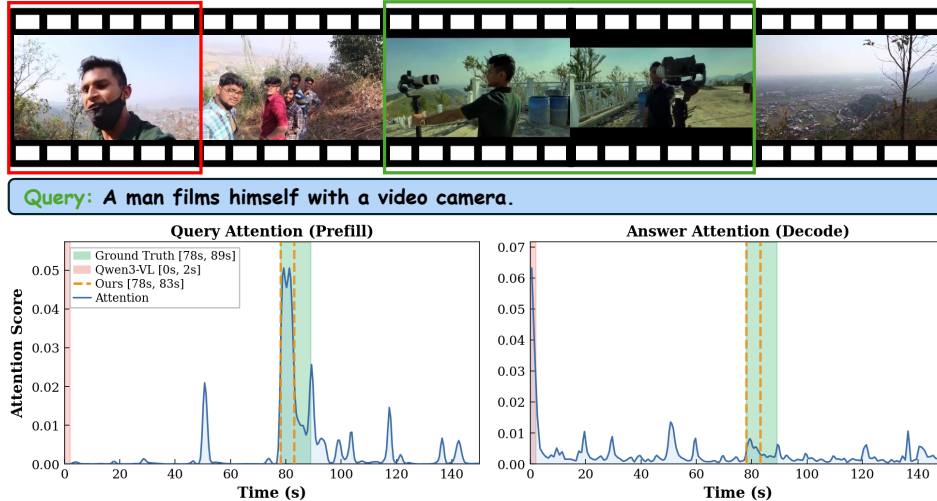


Figure 7: Additional motivation example. Query attention (prefill) sharply peaks at the ground-truth interval, but answer attention (decoding) is overwhelmed by the attention sink at the beginning of the video, causing the baseline to mispredict.

visual-token budget B . For Qwen3-VL-based backbones (Qwen3-VL and TimeLens-8B), the encoder uses a spatial patch downsample rate of 32; for MiMo-VL-7B and Qwen2.5-VL-based backbones, the rate is 28. If the sampled sequence exceeds B , the processor automatically subsamples frames to fit the budget. We use FPS = 2 and $B = 14,336$ visual tokens for every backbone and every benchmark, matching the configuration adopted by TimeLens. Per-model and per-dataset values are listed in Table 9.

Decoding. All predictions (the Stage 1 baseline, the Stage 2 re-inference, and all ablations) are produced with greedy decoding, temperature 0, and at most 64 new tokens. We extract the two floating-point timestamps from the decoded string with a simple regular-expression matcher, following the same post-processing used by TimeLens.

Hardware and software. All experiments are conducted on a node with $8 \times \text{H20}$ GPUs. Stage 1 attention extraction, the zero-video forward pass, and Stage 2 re-inference are all run on a single GPU with batch size 1; the test set is sharded across the 8 GPUs for parallel evaluation. We use PyTorch with SDPA attention kernels; our attention-extraction and attention-mask implementations are written as light-weight monkey patches over the SDPA call so that they incur no additional GPU memory beyond the baseline forward pass.

TG-Head identification. For each backbone we run the attention-knockout procedure of Section 3 once on a held-out subset of 500 samples uniformly drawn from TimeLens’s 100K training corpus [37]. The resulting top-5 heads are then fixed and reused on all three benchmarks without any dataset-specific tuning; the specific layer-head indices for each model are reported in Appendix H.

C Comparison with Other Training-Free Methods

To further contextualize our approach, we compare with two representative training-free VTG methods on QVHighlights-TimeLens using Qwen3-VL-8B as the backbone for all methods. Results are reported in Table 4.

Moment-GPT [31] converts VTG into a text-matching problem: it first generates per-frame captions with an image captioning model, then produces segment-level captions with a video captioning model, and finally scores the similarity between query text and segment captions to select the best temporal span. In our reproduction, we replace both the image captioner and the segment captioner with Qwen3-VL-8B to ensure a fair comparison under the same backbone. As shown in Table 4, this caption-then-match pipeline performs substantially below the direct decoding baseline (49.8 vs.

Table 4: **Comparison with other training-free methods** on QVHighlights-TimeLens. All methods use Qwen3-VL-8B as the backbone. Moment-GPT’s captioning models are also replaced with Qwen3-VL-8B for a fair comparison.

Method	R1@0.3	R1@0.5	R1@0.7	mIoU
Baseline	74.1	64.1	49.1	59.4
Moment-GPT [31]	66.5	56.1	37.9	49.8
NumPro [28]	74.3	64.5	49.0	59.6
Ours	77.3	67.0	51.2	61.9

59.4 mIoU). The bottleneck is that converting continuous visual content into discrete text captions inevitably discards fine-grained temporal information, and errors in caption generation propagate to the matching stage, leading to imprecise boundaries.

Number-Prompt (NumPro) [28] overlays a visible frame number onto each video frame and asks the MLLM to “read” the temporal position via its OCR capability. This approach was shown to be effective on earlier MLLMs that lacked explicit temporal encoding. However, modern MLLMs such as Qwen3-VL already interleave textual timestamp tokens before each frame’s visual tokens, providing the model with an explicit sense of time without relying on visual watermarks. As a result, adding frame-number overlays to Qwen3-VL yields negligible improvement over the baseline (59.6 vs. 59.4 mIoU). The timestamp mechanism built into the model architecture already subsumes the information that NumPro attempts to inject visually.

These results suggest that earlier training-free techniques were designed around the limitations of weaker MLLMs (e.g., lack of temporal encoding or poor direct grounding ability). In contrast, our method reads the model’s *internal* attention signal rather than manipulating the *external* input (captions or visual watermarks), and achieves a much larger improvement (+2.5 mIoU) without modifying the video content or the prompt format.

D Why We Need Entropy-Based Attention Aggregation

The query sentence contains tokens with very different temporal discriminativeness. Figure 8 visualizes the per-token attention curves of a single TG-Head for the query “A man is exercising beside a car”. Function tokens such as “A” distribute attention almost uniformly across the entire video, producing a high-entropy curve that is dominated by the attention sink at the very beginning and by generic background noise. Tokens that repeatedly appear across frames such as “man” are also noisy: the model attends to multiple people in the video, not only the target man. In contrast, content tokens that are specific to the queried action or object, such as “exercising” and “car”, produce sharp peaks inside the ground-truth interval (low entropy), accurately highlighting the event of interest.

A naive approach that simply averages all per-token attention curves would be dominated by the noisy, high-entropy tokens that contribute most of the energy but none of the temporal discriminativeness. Our entropy-based weighting inversely prioritizes low-entropy (i.e., concentrated) tokens, which effectively suppresses the noise from function words and frequently-occurring nouns while amplifying the signal from semantically discriminative tokens. This directly translates into more precise interval detection, as reflected in the *Entropy (Ours)* row of Table 3 in the main paper.

E Why We Need Contrastive Attention Debiasing

Even after entropy-based aggregation, the resulting curve still suffers from systematic content-independent biases. The most prominent one is the well-known “attention sink” phenomenon [12]: MLLMs tend to allocate a disproportionately large fraction of attention to the first few visual tokens, regardless of what the query is about. Figure 9 illustrates this effect. The *Positive Attention* curve (top) peaks correctly around the ground-truth interval, but it is accompanied by a tall spurious peak at the very beginning of the video. This spurious peak is purely an artifact of the model’s architectural bias: it is still present when the video is replaced by a blank (all-zero) video, as shown by the *Zero Attention* curve (middle). By dividing the positive attention by the zero attention and keeping only the

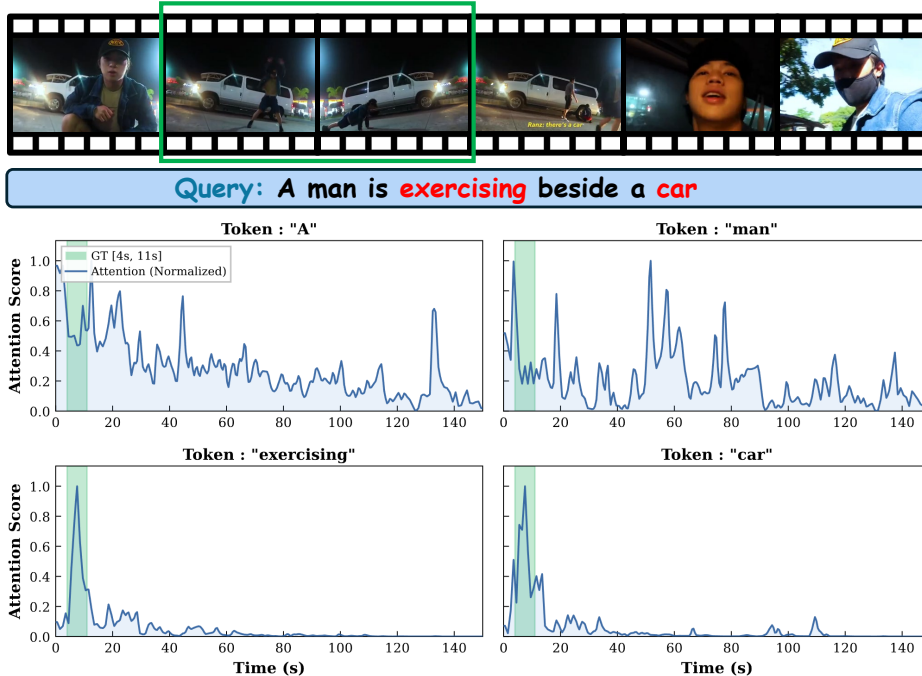


Figure 8: **Per-token attention distributions.** Function and generic tokens (“A”, “man”) yield high-entropy, uninformative curves, while content tokens (“exercising”, “car”) yield low-entropy curves that sharply peak inside the ground-truth interval. Entropy-based weighting prioritizes these informative tokens.

positive contributions, the *Debiased Attention* curve (bottom) removes the attention sink and reveals a clean, query-specific attention signal that can be reliably used for interval detection.

To quantitatively assess the impact of this debiasing step, we compare performance with and without contrastive debiasing on Qwen3-VL-8B across all three benchmarks in Table 5. Without debiasing, the interval detection is frequently dragged toward the beginning of the video by the attention sink, causing a consistent degradation across all metrics.

Table 5: **Ablation on Contrastive Attention Debiasing** using Qwen3-VL-8B. Removing debiasing causes the interval detection to be systematically pulled toward the attention sink at the start of the video, degrading all metrics.

Method	QVHighlights-TimeLens				Charades-TimeLens				ActivityNet-TimeLens			
	R1@0.3	R1@0.5	R1@0.7	mIoU	R1@0.3	R1@0.5	R1@0.7	mIoU	R1@0.3	R1@0.5	R1@0.7	mIoU
w/o Debiasing	75.4	65.0	49.3	60.4	69.6	53.8	28.0	48.6	62.8	51.8	34.9	47.5
w/ Debiasing (Ours)	77.3	67.0	51.2	61.9	71.2	55.2	28.3	49.5	64.2	52.9	35.4	48.2

F Effectiveness of TG-Heads Selection

To validate that the TG-Heads identified by our knockout procedure are indeed the right heads to use, we compare several alternative head-selection strategies on Qwen3-VL-8B (QVHighlights-TimeLens) in Table 6. All variants use the same downstream pipeline (entropy aggregation, contrastive debiasing, interval detection, and Hard Crop re-inference); only the set of heads from which attention is extracted differs.

Two observations stand out. First, using all heads or a random subset of heads actually *degrades* performance relative to the baseline (e.g., All heads: 57.5 vs. Baseline: 59.4 mIoU). This confirms that the vast majority of heads do not carry useful temporal grounding information. Including them injects noise that corrupts the attention signal and misleads the interval detection. Second, the top-5 heads

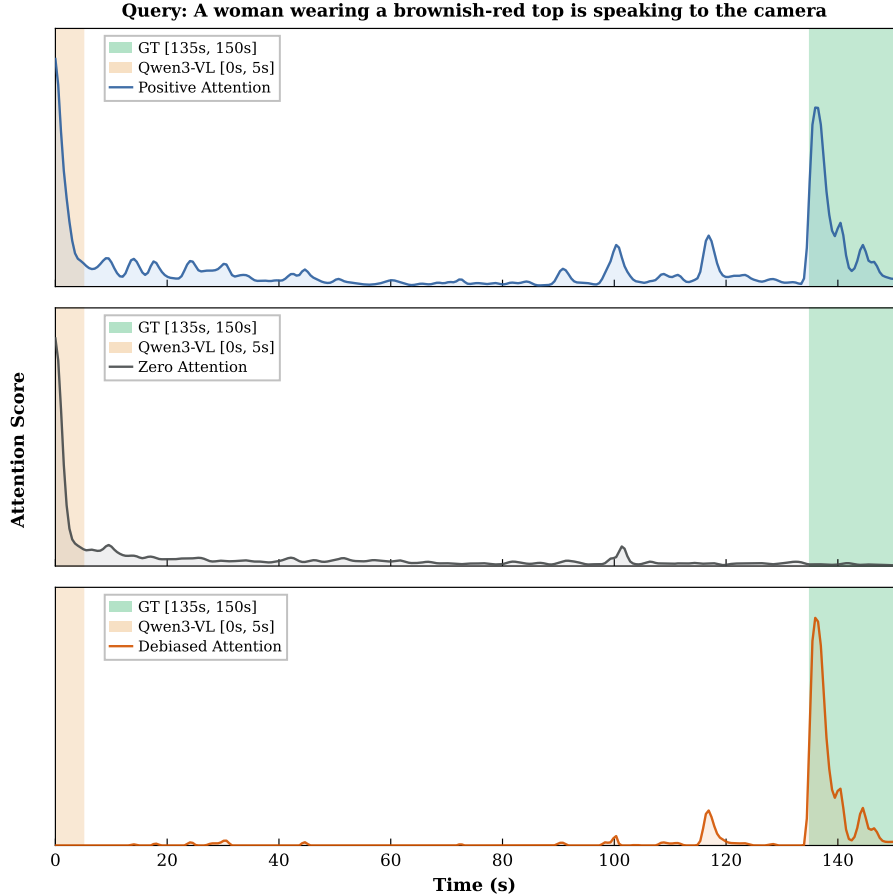


Figure 9: **Effect of contrastive attention debiasing.** **Top:** Positive attention on the real video exhibits both a correct peak near the ground-truth interval and a spurious peak at the beginning of the video (attention sink). **Middle:** Zero attention on a blank video reveals that the beginning-of-video peak is a content-independent bias intrinsic to the model. **Bottom:** After contrastive debiasing, the bias is removed and only the query-specific peak remains.

selected by GCS substantially outperform the next-best tier (Top 5–10), which in turn outperforms the random and all-head baselines. This validates the head knockout procedure as an effective way to isolate the most informative heads and demonstrates that TG-Head selection is critical to the success of our framework.

G Long-Tailed Distribution of TG-Heads

Figure 10 shows the sorted mIoU drops obtained when knocking out each individual head for four different MLLMs. For every model, the curve exhibits a steep initial decline followed by a long flat tail that even yields slight gains at the extreme end. This confirms that the heavy-tailed concentration of temporal grounding capability is not specific to a single architecture: across MiMo-VL-7B, Qwen3-VL-4B, Qwen3-VL-8B, and TimeLens-8B, only a small number of heads are essential for temporal grounding, while the vast majority are either redundant or inert. This long-tailed pattern justifies our decision to select only the top- K heads, with K as small as 5.

H TG-Heads of Different Models

Table 7 lists the top-5 TG-Head indices (layer, head) for each evaluated model. While the specific indices vary across architectures, several patterns emerge. First, TG-Heads consistently appear

Table 6: **Ablation on head selection** (Qwen3-VL-8B, QVHighlights-TimeLens). “All heads” extracts attention from every head in the model. “Random 5” averages five randomly sampled heads (mean over 3 draws). “Top 5–10” uses the heads ranked 6th–10th by GCS. “Top 5 (Ours)” uses the five highest-GCS heads.

Head Selection	R1@0.3	R1@0.5	R1@0.7	mIoU
Baseline	74.1	64.1	49.1	59.4
All heads	72.5	62.2	47.6	57.5
Random 5 heads	73.1	63.5	47.9	58.3
Top 5–10 heads	75.7	65.8	50.1	60.6
Top 5 heads (Ours)	77.3	67.0	51.2	61.9

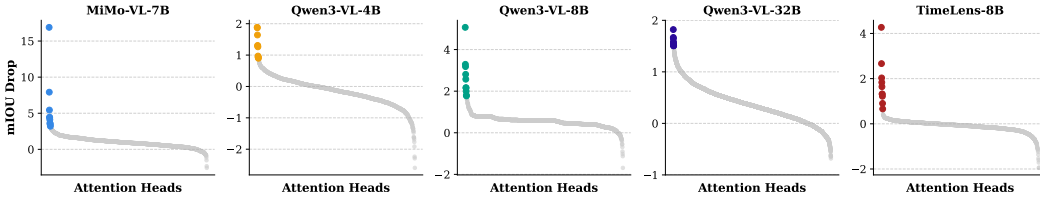


Figure 10: **Sorted mIoU drop curves under single-head pruning** for four MLLMs. The drop is heavy-tailed: the top few heads dominate grounding performance, while the remaining heads are largely redundant or noisy.

in the middle-to-deep layers (layers 15–29 for the 7B and 8B models), suggesting that temporal grounding relies on high-level cross-modal reasoning rather than low-level feature extraction. Second, the identified heads remain stable across different evaluation subsets and datasets, confirming the robustness of the one-time knockout procedure.

Figure 11 further reports the GCS heatmaps for Qwen3-VL-4B and Qwen3-VL-32B, which were omitted from the main paper for space. Both scales exhibit the same long-tailed concentration pattern as the 8B models shown in the main text, and the selected top-5 heads (marked with stars) stand out clearly against the background.

Table 7: Top-5 TG-Head indices for each model.

Model	TG-Head Indices (layer, head)
MiMo-VL-7B	(19, 3), (20, 19), (14, 17), (0, 1), (28, 24)
TimeLens-8B	(15, 8), (18, 22), (15, 0), (15, 2), (17, 24)
Qwen3-VL-4B	(21, 11), (27, 18), (18, 14), (20, 15), (28, 16)
Qwen3-VL-8B	(15, 11), (15, 8), (18, 15), (21, 31), (29, 12)
Qwen3-VL-32B	(19, 54), (43, 52), (23, 40), (33, 60), (2, 40)

I Hyperparameter Settings

Although our framework involves several hyperparameters (Table 8), most of them are fixed to the same default values across all models and datasets. Specifically, the number of TG-Heads K , entropy temperature τ , Gaussian smoothing σ , and threshold ratio ρ are kept constant throughout, as are the frame sampling rate and total visual-token budget. Only two interval-construction parameters, the dilation window δ and expansion ratio r , vary with dataset duration: Charades-TimeLens contains much shorter videos than QVHighlights-TimeLens and ActivityNet-TimeLens, so we use a smaller temporal window and less context expansion for Charades. The Stage 2 variant is fixed by backbone, with Hard Crop used for general-purpose MLLMs and Soft Mask used for the VTG-tuned TimeLens-8B.

The two confidence thresholds are model-level parameters rather than dataset-level ones, because both decode confidence and attention confidence are strongly tied to the calibration of the backbone

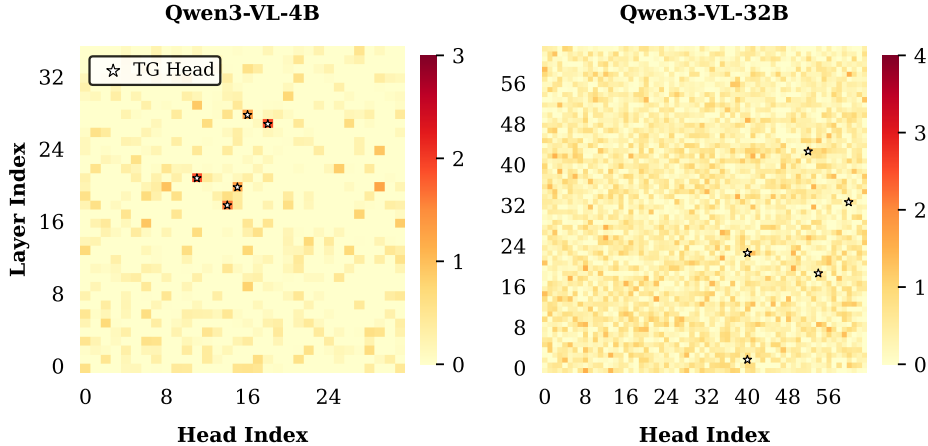


Figure 11: **Grounding Contribution Score (GCS) for Qwen3-VL-4B and Qwen3-VL-32B.** Consistent with the models reported in the main paper, the temporal grounding capability remains highly concentrated in a sparse set of TG-Heads, confirming that this heavy-tailed pattern generalizes across model scales.

itself and correlate with localization accuracy (Figure 5). We select θ_{dec} and θ_{attn} on a validation split of 500 randomly sampled examples from the TimeLens-100K training corpus, and then apply the selected thresholds unchanged to all test sets. No hyperparameter is tuned on the TimeLens-Bench evaluation sets. Table 9 lists the final configuration used to produce the main results in Table 1.

Table 8: **Algorithmic hyperparameters** of our framework, with the symbols used in the main paper.

Parameter	Symbol	Default
Number of TG-Heads	K	5
Entropy temperature	τ	0.5
Gaussian smoothing	σ	2.0
Threshold ratio	ρ	0.2
Dilation window (seconds)	δ	5.0
Expansion ratio	r	0.15
Decode confidence threshold	θ_{dec}	0.9
Attention confidence threshold	θ_{attn}	0.9

Table 9: **Final hyperparameter configuration** used to produce the numbers in Table 1. FPS is the frame sampling rate, “Tokens” is the total visual-token budget, and “Stage 2” is the chosen Stage 2 variant. Most parameters use the defaults in Table 8; only δ and r vary with dataset duration, while the confidence thresholds are selected per backbone on the TimeLens-100K validation split.

Model	Dataset	FPS	Tokens	Stage 2	K	τ	σ	ρ	δ (s)	r	θ_{dec}	θ_{attn}
MiMo-VL-7B	QVHighlights-TimeLens	2	14,336	Hard Crop	5	0.5	2.0	0.2	5.0	0.15	0.9	0.9
	Charades-TimeLens	2	14,336	Hard Crop	5	0.5	2.0	0.2	3.0	0.1	0.9	0.9
	ActivityNet-TimeLens	2	14,336	Hard Crop	5	0.5	2.0	0.2	5.0	0.15	0.9	0.9
Qwen3-VL-8B	QVHighlights-TimeLens	2	14,336	Hard Crop	5	0.5	2.0	0.2	5.0	0.15	0.8	0.9
	Charades-TimeLens	2	14,336	Hard Crop	5	0.5	2.0	0.2	3.0	0.1	0.8	0.9
	ActivityNet-TimeLens	2	14,336	Hard Crop	5	0.5	2.0	0.2	5.0	0.15	0.8	0.9
TimeLens-8B	QVHighlights-TimeLens	2	14,336	Soft Mask	5	0.5	2.0	0.2	5.0	0.15	0.8	1.0
	Charades-TimeLens	2	14,336	Soft Mask	5	0.5	2.0	0.2	3.0	0.1	0.8	1.0
	ActivityNet-TimeLens	2	14,336	Soft Mask	5	0.5	2.0	0.2	5.0	0.15	0.8	1.0

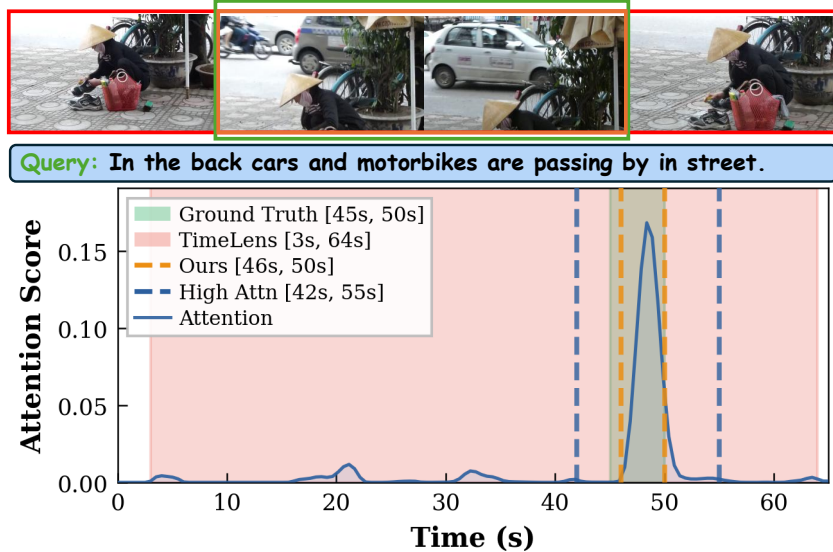


Figure 12: **Successful correction (Example 1)**. The baseline predicts an overly broad interval that covers almost the entire video, while the TG-Head attention concentrates on a narrow high-attention region. Restricting the visual context to this region allows Stage 2 to localize the event much more precisely.

J Efficiency Analysis

Our framework adds two extra forward passes to the baseline single-pass inference: one zero-video pass for contrastive debiasing in Stage 1, and one Stage 2 re-inference pass. Table 10 reports the average per-sample inference time on each benchmark for Qwen3-VL-8B and TimeLens-8B, measured with the confidence gate disabled (i.e., all samples go through both stages) to reflect the worst-case overhead.

For TimeLens-8B, which uses the Soft Mask variant, Stage 2 simply modifies the attention mask and runs a second forward pass on the same input without re-reading or re-encoding the video. The per-sample time is therefore roughly $3\times$ the baseline (one positive pass, one zero-video pass, one masked re-inference). For Qwen3-VL-8B, which uses Hard Crop, Stage 2 requires re-reading the cropped video segment and re-encoding it through the visual encoder, resulting in a somewhat larger overhead.

Note that the timings in Table 10 represent the worst case where every sample enters Stage 2. In practice, the confidence gate skips Stage 2 for a substantial fraction of samples (the “Skip%” column). Skipped samples incur only the baseline cost plus the zero-video pass ($\sim 2\times$), so the effective average overhead is lower than the reported numbers.

Table 10: **Efficiency analysis**. Average per-sample inference time (seconds) with the confidence gate disabled (worst case). “Skip%” is the fraction of samples that would be skipped when the gate is enabled; for these samples the actual cost is only $\sim 2\times$ baseline. Measured on a single H20 GPU with batch size 1.

Model	QVHighlights-TimeLens			Charades-TimeLens			ActivityNet-TimeLens		
	Baseline	+Ours	Skip%	Baseline	+Ours	Skip%	Baseline	+Ours	Skip%
Qwen3-VL-8B	3.8 s	15.9 s	89%	2.8 s	11.7 s	83%	3.6 s	17.1 s	91%
TimeLens-8B	3.8 s	11.6 s	80%	2.8 s	8.5 s	94%	3.6 s	11.0 s	91%

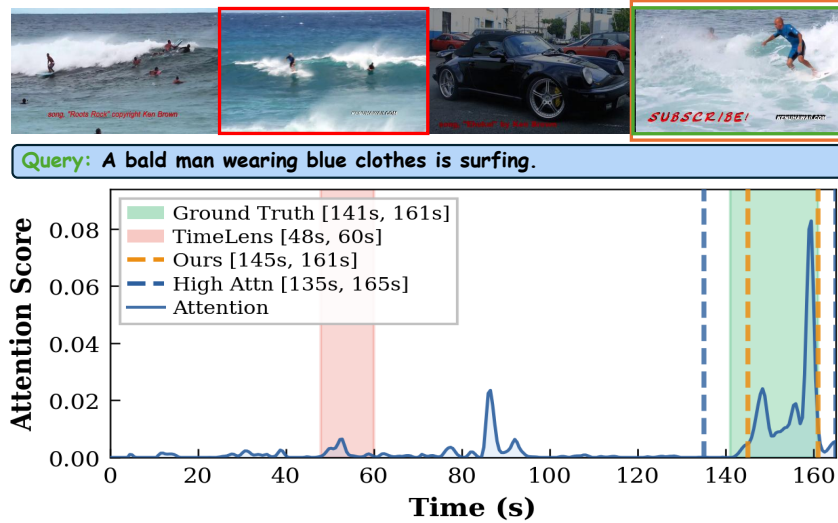


Figure 13: **Successful correction (Example 2)**. The baseline produces an inaccurate interval, while our method tightens it around the true event by leveraging the clean prefill attention signal.

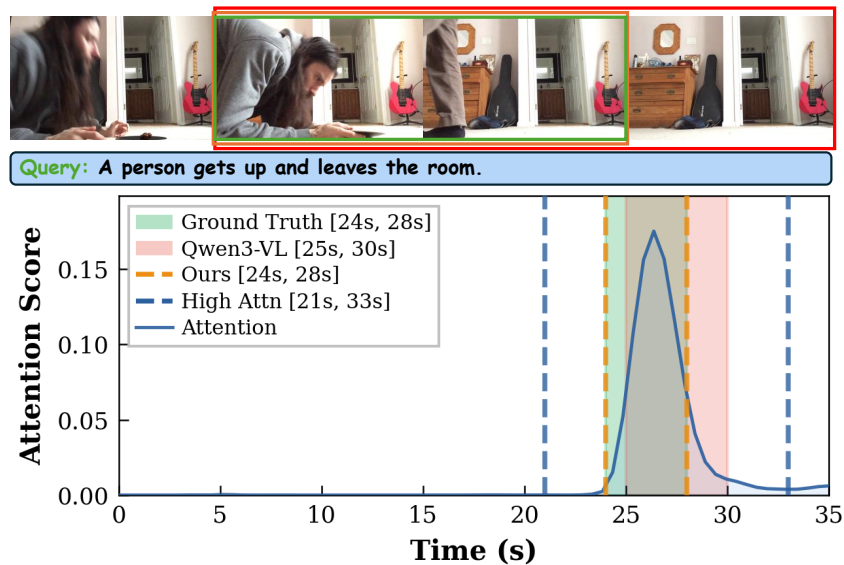


Figure 14: **Successful correction (Example 3)**. The baseline already overlaps substantially with the ground truth but remains imprecise. By cropping to the high-attention interval, Stage 2 reduces the number of frames and increases per-frame resolution, yielding a prediction that aligns exactly with the ground-truth interval.

K More Successful Examples

We provide additional qualitative examples beyond those in the main paper. Example 1 shows that our method can tighten an overly broad baseline prediction by focusing on the narrow high-attention region. Example 3 further shows that even when the baseline substantially overlaps with the ground truth, cropping to the high-attention interval can improve temporal precision by increasing the effective per-frame resolution.



Figure 15: **Failure case 1 (multi-peak)**. The query mentions a “small plastic bowl” that appears at two separate moments. Stage 1 correctly picks the later peak (ground truth), but the detected high-attention interval encompasses both peaks and Stage 2 is pulled to the earlier, higher-amplitude one.

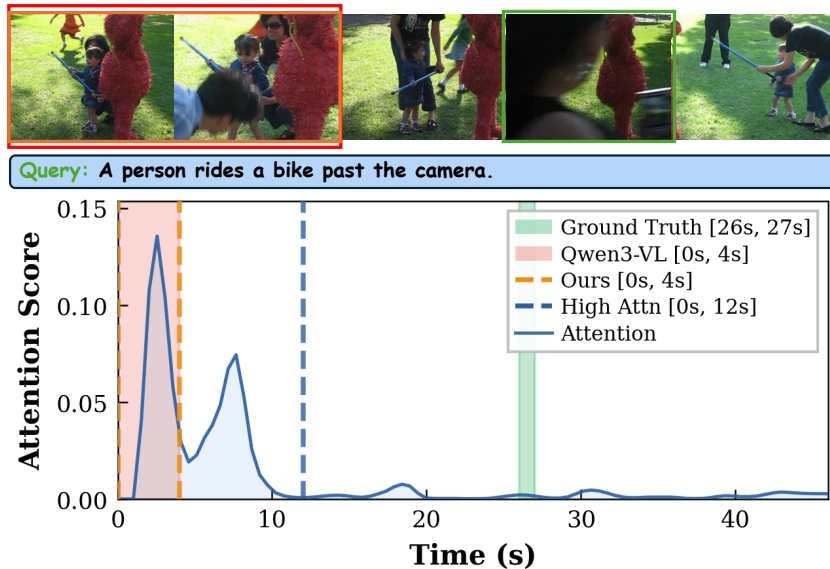


Figure 16: **Failure case 2 (absent attention at GT)**. The ground-truth interval receives near-zero attention, while both the baseline and our method predict a high-attention but incorrect segment. When TG-Head attention does not correlate with the ground truth, our framework cannot provide a correction.

L Failure Cases

While our framework consistently improves average performance, there are individual samples on which it fails to help or even slightly hurts the prediction. We present two representative failure modes below.

The first mode (Figure 15) is the multi-peak case discussed in the main paper: a queried object or action recurs at several moments in the video, producing multiple attention peaks. The high-attention interval merges these peaks, and Stage 2 can be pulled toward the wrong one even though Stage 1 happened to pick the correct peak.

The second mode (Figure 16) is more fundamental: the ground-truth interval itself receives little or no attention from the TG-Heads. In this case, the attention curve peaks at a different segment that is visually salient but does not correspond to the queried event. Both the baseline model and our method are drawn to this high-attention but incorrect interval, because our framework fundamentally relies on the assumption that TG-Head attention correlates with the ground truth. For the small fraction of samples where this assumption fails, our method cannot provide a correction.

M Limitations and Future Work

Limitations. Our framework has two main limitations. First, the high-attention interval detection assumes the query corresponds to a single contiguous temporal region. This matches the current standard VTG benchmarks, which are all single-interval, but may not generalize to multi-interval settings. Even within single-interval benchmarks, when a key object or action recurs at several moments in the video (see Appendix L for concrete examples), our detector may merge the peaks and Stage 2 may be pulled toward the wrong one. Second, the framework adds extra forward passes on top of baseline inference: one zero-video pass for bias estimation, and one Stage 2 pass for samples that the confidence gate does not skip. This increases per-sample inference time by roughly $3\times$ for the Soft Mask variant and up to $4\times$ for the Hard Crop variant (see Appendix J), which is acceptable for offline evaluation but may be non-trivial for latency-critical applications.

Future work. Three directions seem particularly promising. (i) *Multi-interval detection.* Extending our detector to return multiple candidate intervals and letting Stage 2 evaluate each of them would address the multi-peak failure mode discussed above. (ii) *Beyond temporal grounding.* The perception-generation gap we observe is not specific to VTG; similar patterns have been reported on visual question answering [22, 36]. We plan to explore whether the same “read-then-regenerate” recipe can improve other tasks such as dense video captioning, temporal action detection, or even spatial grounding in images. (iii) *Merging Stage 2 with post-training.* It would be interesting to study whether explicitly supervising a post-trained model with the attention signal that Stage 1 extracts (rather than only with the ground-truth timestamps) can give the model more concentrated TG-Heads and thus make it better suited to our framework.